SPECTRAL ANALYSIS USING A MULTI-BIN METHOD FOR PHOTOVOLTAIC SITES

Elijah L. Maweza[1], Lawrence Pratt[1] and Kittessa Roro[1]

,[1]Council of Scientific and Industrial Research, Pretoria, South Africa, CSIR-Energy Centre, E-mail: lmaweza@csir.co.za

CSIR Energy Centre, Pretoria, South Africa E-mail: lpratt@csir.co.za

[1]CSIR Energy Centre, Pretoria, South Africa, E-mail: kroro@csir.co.za

Abstract: The high demand for low carbon energy and rapidly decreasing solar panel prices have led to a surge in solar photovoltaic (PV) plants across the globe, more than at any other time since the industry began. Combined with geographic variations in environmental conditions, this has led to a vast increase in the need for characterisation of local spectral data. However, obtaining site-specific spectral data can be difficult for average users due to their high cost, varying accuracy, and difficulty to operate and maintain.

Currently, users work with spectral data obtained from the American Society for Testing and Materials (ASTM) standard, satellites, and the Simple Model for Atmospheric Transmission of Sunshine (SMARTS) Model. To describe spectra generated by any of the above-mentioned sources, researchers have used average photon energy (APE) and other parameters. In this paper, we develop a method for describing PV site-specific clear sky 12-noon spectral data based on environmental conditions and spectral properties. The approach bins measured spectra into 100 and 200 nm wavelength ranges and characterises their changes throughout the year with the plane of array (PoA) irradiance, APE, air mass (AM) and sun elevation at the site to establish relationships.

The method developed showed strong correlations between the APE and the PoA irradiance, the AM and the sun elevation in three clear sky days, each month over the period of three years. The observed strong correlations between these parameters indicate that when spectra cannot be measured, the measurable site's environmental conditions can help determine the spectral content with strong confidence.

Keywords: Air mass; Sun elevation; Plane of array irradiance; Spectral distribution; Binning, Average photon energy.

1. Introduction

The growing demand for clean energy over the past decade has resulted in a rapid increase in cumulative installed PV electricity generation capacity, while the price of PV modules has decreased more than expected. By the end of 2012, the cumulative installed capacity reached 100 GW, but reached 635 GW by 2019 as a result of increased installations in response to increased demand [1]. Further growth forecasts predict several tens of terawatts PV capacity will be achieved before 2050 but will require large investments [3]. Parallel to this, electric energy generation from solar PV depends on the environmental conditions and solar energy received. Both factors, together with the spectral irradiance and meteorological parameters such as the ambient temperature and wind speed, all differ seasonally and also geographically, thus influencing the performances of deployed solar system [2]. The enormous investment in PV systems (conventional and new technologies) has led to a matching economic drive to ensure the best PV sites and most suitable spectrally sensitive PV technologies are chosen for new installations [3].

For high and sustainable energy generation, a PV site requires an abundance of the sun's energy and its seasonal availability [3]. In particular, quantifying the localized spectral irradiance has become topical and key for characterizing and estimating the energy yield of PV devices [4]. However, PV site specific spectral irradiance data are scarce because of the high global standards of precision and cost of instrumentation [5], operation and maintenance [6]. As a result, broadband spectral irradiance data generated by international companies, as well as satellite and model generated spectral data have become an alternative. However, this data overlooks the impact of the angle of incidence and/or the spectral distribution of a specific site and

may lead to impractical yield calculations [7]. Efforts across the world are underway to acquire spectrally-resolved irradiance and site specific data for long term parameter analysis [4]. Binning and long term data analysis are spectral analysis approaches that are increasingly utilised. For example, binning with statistical analysis was conducted on spectral distributions, where APE bins of 0.02-eV and their standard deviations across all 50-nm bands over the wavelength range (350–1050 nm) is divided [2]. Also, long term spectral impact analysis in a PV site was done for PV sites in which they found that the short and long term parameter behaviours may differ [8]. In this research, parameters of interest such as the prevailing environmental conditions, sun position, airmass, plane of array irradiance, and the spectral irradiance were investigated for a long term (three years) because of their direct effect on the performance of solar systems.

The paper compares the spectral distribution of the ASTM global tilt spectrum to the locally measured spectral irradiance under the prevailing environmental conditions. The tests were conducted on three clear sky days a month over the three-year period, from 2018 to 2021, at noon each time. To quantify the variations throughout each of these years, spectral analysis was performed on wavelength bins of 100 nm from 300 to 900 nm and 200 nm from 900 to 1100 nm. For each bin, we determined the APEs to examine how variations during the year relate to other factors.

2. Research Background

2.1. The Influence of the PV Site Geographical Location

The geographical location factors that are unique to a PV site and affect the amount of available solar irradiance and its characteristic spectral distribution are the latitude (determines the airmass) and height above sea level (determines the atmospheric pressure)]. Latitudes and longitudes, indicate how far north (+) or south (-) from the Equator and how far east (+) or west (-) from the Greenwich line is the location respectively.

Solar energy received at a PV site is known to vary due to Earth's continuous rotation around its axis and revolving around the sun, thus changing its tilt around its own axis and giving rise to nights and days and to different seasons of the year respectively. As a result, the duration of nights and days, as well as the relative position of the sun differ. At the certain times during this process, each of its Earth's hemispheres passes the summer and winter solstices as well as the equinox points in time as shown in Fig. 1. At the summer solstice point, the hemisphere is tilted maximally towards the sun, experiences the longest day of the year and receives high solar irradiance as the sun elevation reaches the highest. Simultaneously, the other hemisphere reaches the winter solstice at the maximum tilt away from the sun, experiences shortest day of the year and receives low solar irradiance. Either of the north or south poles get 24 hours of daytime simultaneously due to refraction, while the other goes through 24 hours of night time. This occurs at about June 21 or 22 and December 21 or 22. Equinox is midway between the two solstices, where the Earth's axis of rotation reaches the perpendicular position relative to the Sun (at about March 19–22 and September 21–24) and both hemispheres experience equal durations of night and day and receive equal amounts of solar irradiance[2]. Also, on these dates, both north and south poles get 24 hours of daytime interchangeably due to refraction [2].

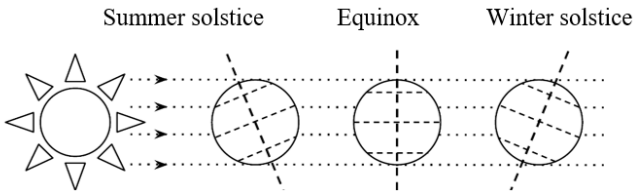

Fig. 1. The Earth's tilts during the summer and winter solstices as well as the equinox.

It is also important to note that when the northern hemisphere experiences the summer solstice, the southern experiences the winter and vice versa.

2.2. Airmass and spectral characterisation

Airmass has an impact on the spectral properties of radiation and in turn the performance of PV systems [3]. Equation (**1**) mathematically defines the airmass as a function of the sun elevation angle. It is the relative atmosphere through which the unscattered solar irradiance crosses from the sun to the ground (the measurement point) [4].

$$AM = \frac{1.0}{(\cos(90^{\circ} - elev) + 0.50572 \times (6.07995 + elev)^{-1.6364})} \quad (1)$$

where *elev* is the solar elevation (º), as observed from the measurement point, defines an angle the sun makes above horizon (0 º) [5] and is inversely proportional to the *AM*.

At standard test conditions (STC), which include the total irradiance of 1000 W/m^2, the airmass of AM1.5 and temperature of 25°, ASTM Gl73 reference spectra (shown later with the measured spectra) are developed [6], namely, the extra-terrestrial, direct and circumsolar as well as the global tilt. The latter is mostly used as an international standard to design all PV modules. This however differs with the real life conditions.

2.3. Characterising spectra

Fig. 2 shows ASTM Gl73 reference spectrum showing three spectra, the extra-terrestrial, direct and circumsolar, and the global tilt. The global tilt spectrum is used as the international

standard when characterizing PV modules at standard test conditions (STC). The light source for solar simulators used during STC measurements should conform closely to the global tilt reference spectrum. The spectral match between the simulated light and the global tilt spectrum is determined by evaluating the percentage of total irradiance in 100 and 200 nm wavelength bins. The STC also requires 1000 W/m^2 light intensity and 25 °C cell temperature.

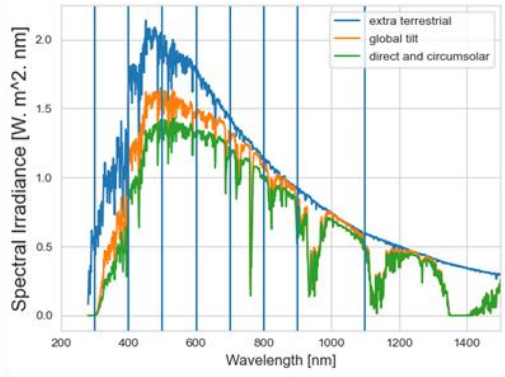

Fig. 2. The ASTM Gl73 reference spectrum showing three spectra, the extra-terrestrial, global tilt and direct and circumsolar spectra [6].

However, the actual operating conditions differ from STC depending on the location and the season of the year. Instead, the locally measured spectra can be useful and when characterised using the average photon energy (APE), spectra can be shown to be "blue" or "red dominant" and used to determine its impact on the annual energy yield of PV technologies. The APE is calculated by dividing the integrated incident irradiance by the integrated photon flux density, and is defined by Equation (**2**)

$$\text{APE}=\frac{\int_a^b E_\lambda(\lambda)d\lambda}{q\int_a^b \varphi(\lambda)d\lambda} \qquad (2)$$

where q [eV] is the electron charge, $E_\lambda(\lambda)$ [W m^{-2}nm^{-1}] is the spectral irradiance at wavelength λ, and φ(λ) is the photon flux density at wavelength λ. The APE values indicate the average distribution of light over the spectrum, regardless of the absolute intensity of light. The average photon energy (APE) is also technology independent parameter and describes only the spectral composition of solar irradiation [7].

The density of the photon flux, φ(λ) is defined by Equation (**3**)

$$\boldsymbol{\varphi_\lambda[photons\, m^{-2}s^{-1}nm^{-1}] = \frac{E_\lambda}{hc/\lambda}} \qquad (3)$$

which is calculated using the Plank–Einstein relation $\boldsymbol{hc/\lambda}$ [J]. It is the number of incident photons per unit area per second per wavelength.

3. Methods employed in data collection and analysis

3.1. Obtaining the Airmass And Solar Elevation Values.

The airmass is one of the major environmental properties used to characterize the measurement site. Its data was sourced together with the site specific zenith angle, elevation, and azimuth angle of the sun from the online available Solar Geometry Calculator developed by the NOAA Earth System Research Laboratories (ESRL) [8]. To obtain the site specific data, the calculator requires the correct location coordinates, namely, the latitude and longitude as well as the timescale of the measurement site and can access historical data of any range of dates interest.

3.2. PV Testing Site Multi-year Global Irradiance and Spectral Measurement Systems

Fig. 3 shows the outdoor irradiance (top) and spectral (bottom) measurement systems mounted on a dedicated weather station on the roof of Building 34 on the CSIR Pretoria campus.

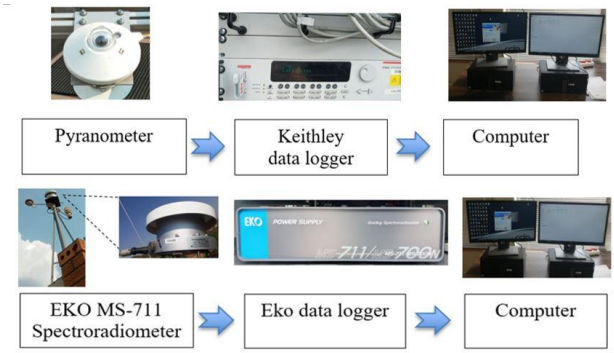

Fig. 3. Top: data acquisition system to measure the plane of array Irradiance. Bottom: The spectral data acquisition system to measure the spectral data

The irradiance measurement system includes the pyranometer and Keighley data logger, while the spectral measurement system includes the new generation grating MS 711 spectroradiometer and the EKO data logger. Both the pyranometer and the spectroradiometer are mounted in the same plane and environment conditions, taking continuous measurements of plane of array (PoA) irradiance and spectrum, respectively. The devices are unique, robust, with no moving parts, and suitable for most weather conditions. The spectroradiometer in particular, operates optimally in the temperature range of -10 ºC to 50 ºC and records spectra in the 300 nm to 1100 nm wavelength range with an accuracy of +/- 0.2 nm [9].

3.3. Data pre-processing

For our investigation, three clear sky days with high PoA

irradiance were selected for every month over the test period from 2018 to 2020. The data includes the measured spectra, the measured PoA irradiance, the site location, calculated air mass and calculated sun elevation on the site. The seasonal and hourly variations of these parameters at 12-noon is characterized.

The spectral measurements were assigned to bins corresponding to the IEC 60904-9 standard bins for evaluating spectral mismatch in solar simulators [10]. Specifically, the spectra were binned from 400-500 nm, 500-600 nm, 600-700 nm, 700-800 nm, 800-900 nm and 900-1100 nm wavelengths. The relative energy distribution in each bin was then calculated to determine their percentage contribution to the integrated spectral irradiance and help characterize the shifts in spectrum over the seasons of the year.

4. Results and discussion

The results of this work are presented to show and interpret the clear-sky variations of the 12 noon environmental conditions, irradiance and solar spectra that characterize a measurement site on a daily and seasonal basis. First, we present air mass, sun elevation, and PoA irradiance variations at the CSIR measurement site on three clear sky days of every month of the year. This is followed by the Eko Spectra data, percentage spectral distribution, and correlation among all the parameters.

4.1. The Air mass and Elevation that characterizes the measurement site

Fig. 4 shows the airmass and sun elevation at 12-noon on the actual dates the selected spectral measurements were taken. The airmass and the elevation were obtained using the NOAA solar calculator. These two parameters vary by inverse proportion throughout the year following Equation (1). At higher sun elevation, lower air mass is observed and vice versa. This directly affects how much solar energy is maximally available at each specified period [2], as well as the corresponding spectra.

The airmass ranges from the shortest AM1.0 in December 26 (summer) to the longest AM1.53 in in June 16 (winter), exactly when the sun elevation is the highest at 87.2º and the lowest at 40.9º respectively. This indicates that the standard airmass AM1.5 used when testing solar modules is only realized in winter months in Pretoria.

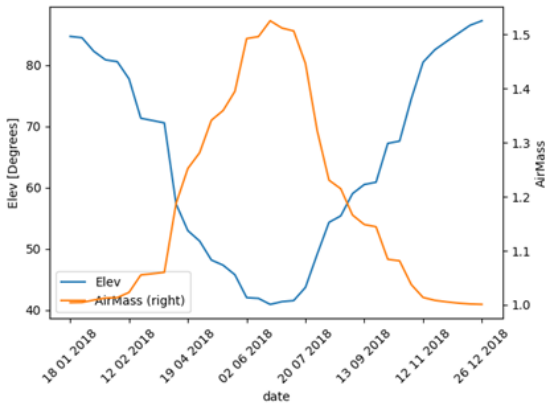

Fig. 4. The 12 noon air mass and the sun elevation at the CSIR corresponding to spectral measurement dates

4.2. Lists CSIR PV testing site multiyear global irradiance

Fig. 5 shows hourly trends of the PoA irradiance (25° tilt, 0° azimuth) measured at the CSIR around solar noon by month. For each plot, three clear sky days with the highest values at 12-noon were selected in each month from 2018 to 2020. The horizontal dotted line represents the STC 1000 W/m^2 plotted here to show visually how the PoA irradiance vary throughout the year.

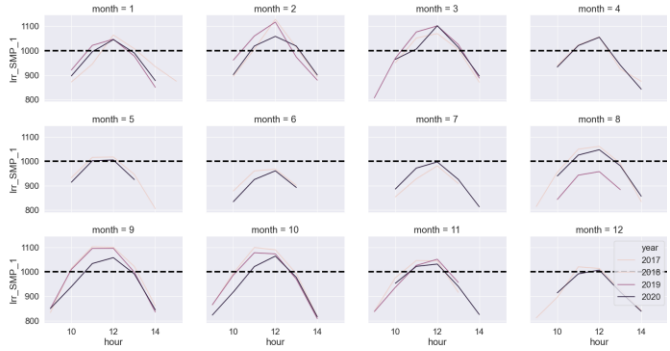

Fig. 5. Average hourly PoA irradiance near solar noon for each year by month

The highest irradiance values (~1100 W/m^2) were measured during the months of February and March as well as September and October around the spring and autumn equinox when the sun position is nearly perpendicular to the plane of array at solar noon. The lowest values (~950 W/m^2) were measured during June when the sun elevation is low in the sky, which are the days close to the winter solstice.

4.3. Combined multi-year spectra and energy distribution for the CSIR PV testing site

This section investigates how the spectra and the energy distributions vary at whole spectra and bin levels over the three-year test period.

Fig. 6 shows the measured spectra over the test period. The spectra are colour coded according to month in each season, with

the vertical lines dividing the spectra into bins. Measured spectra coloured by month/season: black/winter, yellow/summer, green/spring, grey/autumn. The bins in the short wavelength (300 to 600 nm) represent the blue region, medium wavelengths (600 to 900 nm) represent the red region, and long wavelengths (900 to 1100 nm) represent the near infra-red regions of the light spectrum. The spectra plot shows the winter months (black) at the bottom and the summer months (yellow) at the top. The autumn (grey) spectra generally fall nearer to the summer spectra while the spring (green) generally fall nearer the winter spectra. The up and down shifts observed in this diagram are indicative of the variation of light intensity when the spectrum was measured, not a shift in spectral distribution.

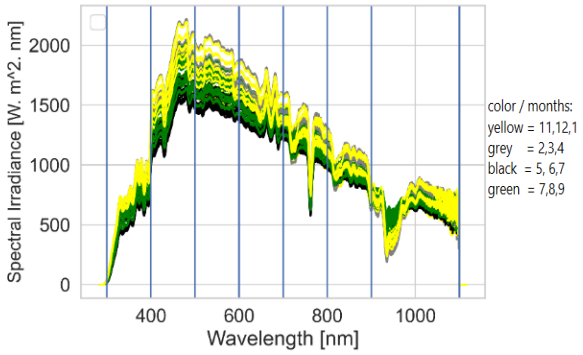

Fig. 6. Measured spectrum coloured by month/season: black/winter, yellow/summer, green/spring, grey/autumn

To see the left (red) or right (blue) shifts in spectral distributions, the binned data will be analysed in the following diagram.

At bin level, Fig. 7 shows the percentage of energy variation in each bin, averaged by month. At this level, the spectral energy variations that could not be observed in Fig. 6. Measured spectrum coloured by month/season: black/winter, yellow/summer, green/spring, grey/autumn

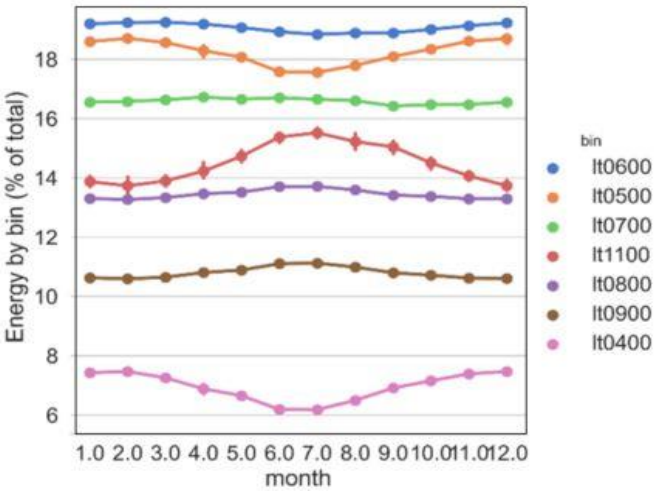

Fig. 7. Energy distribution by month

For example, this significant vitiations of energy distributions in bins lt0500, lt1100 and lt0400 and minor variations in bins lt0600, lt0700, lt0800 and lt0900 can be observed.

Considering the spectral energy distribution among the bins, the top line shows that roughly 19% of the total energy in the measured spectrum falls in the 'lt0600' bin, i.e. the wavelengths between 500 nm and 600 nm. The variation from month to month is small for this bin. However, the energy in the 'lt0400' bin, i.e. the wavelengths between 300 and 400 nm, is higher in summer compared to winter. By contrast, the energy in the 'lt1100' bin is lower in summer compared to winter. This indicates that during summer months, the spectra contain a higher percentage of total energy in the blue region and a lower percentage of total energy in the red region compared to winter months. The percentage of total energy in the 600-800 nm wavelengths remains relatively stable throughout the year. Based on analysis of the binned energy, the data show a measurable shift from blue in the summer months to red in the winter months.

4.4. Spectral bin correlation with spectral, irradiance and environmental properties

Visualizing the relationships among the spectral bin energy distributions and other parameters, reveals correlations that can be analysed. Fig. 8 shows multi variant pairs plots, where each bin (here represented by lt0400 and lt0900) is plotted against itself, selected bins, as well as other parameters such as months, PoA irradiance (Irr_SMP_1), airmass (Airmass), sun elevation (Elev) above the horizon and APE (ape). The bins' energy distribution and the APE characterize the measured spectra while other parameters present the months when measurements were taken, and describe the environmental conditions of the PV site.

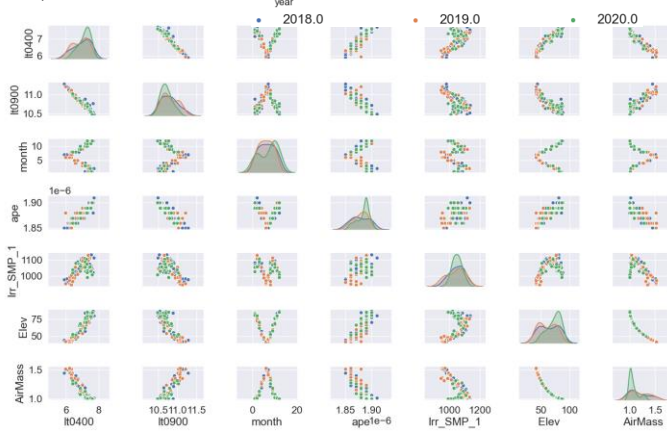

Fig. 8. Multivariable pair plots involving the spectral bins, air mass and irradiance for the three years in question.

The pairs plots show density plots along the diagonal and the scatter plots elsewhere to help identify trends for further analysis. The density plots, in particular, illustrate the distribution of a single variable while the scatter plots

demonstrate the existence or non-existence of relationships between any two of the considered variables. The diagonal density plots behaviour varies from left skewness at top left (short wavelengths) to right skewness at bottom right (longer wavelengths) indicating that the mean is to the left and to the right of the peak respectively with minor differences among the different years. In the lt0600 and lt0700 bins, the density plots are in the middle.

Among the scatter plots, the first row where lt0400 (300 to 400 nm) bin is selected to represent the blue region and plotted against the lt0900 bin which represents the red region, and also with other parameters. It was observed that lt0400 has weak positive and negative correlations with the lt0600 and lt0700 bins respectively. This indicates that the transition of correlation between lt0400 with other bins from positive to negative occur between the lt0600 and lt0700 bins. This also explains why a minimum to no variation of percentage energy distribution was observed in the lt0600 and lt0700 bins in Fig. 7. These bins are not shown in Fig. 8 so that we can clearly show the bins that represent the blue and red region bins with clarity. For example, with the lt0900 (800 to 900) bin, lt0400 has a negative correlation with high linearity, indicating that when the energy in the blue region is high, the energy in the region will be low. With the months' variable, the lt0400 bin values are high during the summer months (the beginning and end of the year), but decrease in the intervening months to reach the minimum in winter. With other parameters, the lt0400 bin has a negative linear correlation with air mass and positive correlations with the plane of array irradiance, sun elevation and APE.

The lt0900 bin, which represents the red region of the spectra in the pairs plots, correlates negatively with the blue region bins, has low values in the summer months and high values in the winter months. The bin has no clear correlation with the plane of array irradiance, negative correlations with the sun elevation and the APE and a positive one with air mass. The months' variable, when plotted against the plane of array irradiance shows the same effect observed in Fig. 5, where high values were obtained in February and March and September and October, which are the months close to the Equinox dates. The opposite behaviour between air mass and sun elevation shown in Fig. 4 is illustrated in Fig. 7 in rows two and three from the bottom and the second and third column from the right, as a non-linear (near logarithmic) negative correlation.

5. Results and discussion

The spectral distribution of solar irradiance is unique to the measurement site of interest. It varies hourly from sunrise to sunset in a day and seasonally from January to December because of the differences of prevailing weather conditions (e.g. cloudy or clear sky). To solve the scarcity of site specific spectral data, CSIR commissioned a spectroradiometer and a pyrometer mounted in dedicated weather stations on site to measure spectral and irradiance content. Following this, we characterized the spectral distribution using the APE and spectral binning.

Midday spectral distribution measured at the CSIR campus in Pretoria varies seasonally throughout the year due to the changes in sun position and the related. In this work, we analysed two or three 12 noon spectra for clear sky days, in every month of the years 2018 to 2020. First, we established the environmental properties of the measurement site to confirm that the midday sun elevation is lower in winter compared to summer and the corresponding air mass is higher in winter compared to summer. The spectral measurements were plotted to determine changes in the distribution of energy versus wavelength over the course of the year. The spectral measurements have a visually similar shape throughout the year, while the intensity changes. The minimum intensities were observed in winter months and the maximum intensities were observed in summer months. We then characterized the spectral distribution using the APE and spectral binning. We established a quantitative and traceable variation of the APE which corresponds to the variations observed in the spectra. The low values of APE were observed in winter while in summer high values of the APE were obtained. We then characterized the spectral distribution using the APE and spectral binning. We also established a quantitative and traceable variation of the APE which corresponds to the variations observed in the spectra. The low values of APE were observed in winter while in summer high values of the APE were obtained.

The measured spectra were binned using relative areas under the curve in each bin for every spectrum of the selected days to visualize subtle shifts in the spectral distribution that were difficult to see in full spectral distribution plots. A clear pattern was observed for the short wavelength bins between 300 and 600 nm and the longer wavelength bins between 700 and 1100 nm. In summer months, shorter UV and blue wavelengths make up a higher percentage of the energy in the overall spectral distribution compared to winter. In winter months, longer red and infrared wavelengths make up a higher percentage of the energy in the overall spectral distribution compared to summer. This result confirms a slightly blue shifted spectrum in summer and a slightly red-shifted spectrum in winter.

6. Summary

The study included the analysis of two to three available spectral data for 12 noon in all the months from 2018 to 2020. First, the environmental properties of the measurement site were

established to confirm that midday sun elevation is lower in winter than in summer and the corresponding airmass is higher in winter than in summer. The spectral measurements are visually similar throughout the year, whereas the intensity of the intensity changes. Minimum intensities were recorded through the winter months, while maximum intensities were recorded through the summer months. Following this, we used the average photon energy (APE) and spectral binning to characterize the spectral distribution. We established a quantitative and traceable variation of the APE which corresponds to the variations observed in the spectra. The low values of APE were observed in winter while in summer high values were obtained. We then used the average photon energy (APE) and spectral binning to characterise the spectral distribution. Furthermore, we established a quantitative and traceable variation of the APE which corresponded to variations observed in spectra used.

The measured spectra were binned using relative areas under the curve in each bin for every spectrum of the selected days to visualize subtle shifts in the spectral distribution that were difficult to see in full spectral distribution plots. A clear pattern was observed for the short wavelength bins between 300 nm and 600 nm and the longer wavelength bins between 700 and 1100 nm as represented by lt0400 and lt100 bins respectively. In summer months, shorter UV and blue wavelengths make up a higher percentage of the energy in the overall spectral distribution compared to winter. In winter months, longer red and infrared wavelengths make up a higher percentage of the energy in the overall spectral distribution compared to summer. This result confirms a slightly blue shifted spectrum in summer and a slightly red-shifted spectrum in winter.

The spectral distribution of solar irradiance is unique to the measurement site of interest. It varies hourly from sunrise to sunset in a day and seasonally from January to December because of the differences of prevailing weather conditions (e.g. cloudy or clear sky). To solve the scarcity of site-specific spectral data, CSIR commissioned a spectroradiometer and a pyranometer mounted in dedicated weather stations on site to measure spectral and irradiance content. The data used in this study was measured with these devices, with APE and spectral binning being used to characterize spectral energy distribution.

Acknowledgements

I would like to express my utmost gratitude to CSIR Energy Centre for an opportunity to conduct this research and the support provided. I also thank the National Research Foundation (NRF) for supporting this research financially.

References

[1] A. Jäger-Waldau, “Snapshot of photovoltaics—February 2020,” *Energies*, vol. 13, no. 4, p. 930, 2020.

[2] T. Nakajima and M. D. King, “Determination of the optical thickness and effective particle radius of clouds from reflected solar radiation measurements. Part I: Theory,” *Journal of Atmospheric Sciences*, vol. 47, no. 15, pp. 1878–1893, 1990.

[3] N. Lindsay, Q. Libois, J. Badosa, A. Migan-Dubois, and V. Bourdin, “Errors in PV power modelling due to the lack of spectral and angular details of solar irradiance inputs,” *Solar Energy*, vol. 197, pp. 266–278, 2020.

[4] H. Winkler, “How local conditions affect solar irradiance and photovoltaic module performance in South Africa,” 2017.

[5] “esrl.noaa.gov.” [Online]. Available: https://esrl.noaa.gov/gmd/grad/neubrew/SolarCalc.jsp?mu=on&sza=on&el=on&az=on. [Accessed: May-2021]

[6] “astm.” [Online]. Available: https://www.astm.org/. [Accessed: Oct-2020]

[7] M. Norton, A. G. Amillo, and R. Galleano, “Comparison of solar spectral irradiance measurements using the average photon energy parameter,” *Solar Energy*, vol. 120, pp. 337–344, 2015.

[8] “esrl.noaa.” [Online]. Available: https://www.esrl.noaa.gov/gmd/grad/antuv/SolarCalc.jsp. [Accessed: Oct-2020]

[9] “eko-eu.” [Online]. Available: https://eko-eu.com/applications/dni-measurements-with-a-pyrheliometer. [Accessed: Oct-2020]

[10] I. E. Commission and others, “Photovoltaic devices—Part 9: Solar simulator performance requirements,” *International Standard IEC 60904-9, Edition*, vol. 2, pp. 3–15, 2007.